metals

MDPI

Article

Effects of $Al_2O_3/TiO_2/Na_2O$ on Lime Dissolution in Steelmaking Slag

Kan Yu, Yanling Zhang *, Shuai Zhang and Ming Gao

State Key Laboratory of Advanced Metallurgy, University of Science and Technology Beijing, Xueyuan Road 30, Haidian District, Beijing 100083, China
* Correspondence: ustbzly1108@163.com

Abstract: The mechanism of lime dissolution in steelmaking slag and the factors that influence the dissolution rate are highly significant in improving the efficiency of the steelmaking process; however, they are yet to be fully understood. Here, the effects of $Al_2O_3/TiO_2/Na_2O$ additives on the dissolution rate of lime and the composition of molten slag were investigated using a rotating cylinder technique. The results indicate that the promotion coefficients at 1400 °C decrease in the order of Na_2O > TiO_2 > Al_2O_3. Furthermore, the CaO dissolution rate and kinetic parameters were calculated, and the lime dissolution mechanisms in the presence or absence of Al_2O_3, TiO_2, and Na_2O were compared. Additionally, the data show that ATN (a mixture with a mass ratio of Al_2O_3:TiO_2:Na_2O = 15:4:3) can be used as a suitable flux in the steelmaking process.

Keywords: $Al_2O_3/TiO_2/Na_2O$; lime dissolution; kinetics; steelmaking slag

1. Introduction

The physical and chemical properties of steel slag have a significant impact on the progress of the steelmaking process and the quality of molten steel. CaO must be dissolved in a liquid phase for its efficient functioning, namely, dephosphorization when in the basic oxygen furnace (BOF) and electric arc furnace (EAF) and desulfurization when in the ladle furnace [1]. Traditional steel slag is based on the CaO–FeO–SiO_2 ternary slag system, which has a high melting point and poor fluidity. To improve the fluidity of the slag, various fluorites (such as CaF_2) should be added during production. However, owing to the significant environmental pollution caused by fluorine-containing compounds, the use of fluorite is increasingly being restricted. Recent studies have shown that red mud-based additives containing Al_2O_3, TiO_2, and Na_2O have a significant fluxing effect on traditional steel slag [2,3]. However, the effects of adding these co-solvents in the early stages of lime dissolution remain poorly understood.

When studying factors that influence lime dissolution, Ban-ya et al. [4] found that a CaO–Al_2O_3–Fe_xO_y flux promoted the dissolution of lime owing to the presence of Al_2O_3, and it could be used as a substitute for a CaO–CaF_2–Fe_xO_y flux. Mukawa et al. [5,6] determined the optimal Na_2O and Al_2O_3 contents for Na_2O–CaO and CaO–Al_2O_3 fluxes, respectively. Moreover, Shimoda et al. [7] proposed that a CaO–Al_2O_3–TiO_2 flux significantly promotes the desulfurization of molten iron owing to its low melting point, as well as its viscosity. Additionally, Lee et al. [8] developed a new type of quicklime (CaO) coated with dicalcium ferrite (2CaO·FeO), which possessed high hydration resistance and could rapidly dissolve in BOF and EAF steelmaking slag. Finally, Hamano et al. [9] found that the addition of CaF_2 and $CaCl_2$ resulted in a high rate of lime dissolution in the slag.

Furthermore, the mechanism of lime dissolution in slag has been studied. Schlitt et al. [10] found that upon increasing the FeO content, the dissolution rate of lime in the CaO–FeO–SiO_2 slag significantly increased. Furthermore, a 2CaO·SiO_2 (C2S) layer formed on the surface of CaO particles, and the dissolution of lime was realized by melting the slag through the cracks in the C2S layer. In the presence of high contents of Fe_2O_3, the C2S and

check for updates

Citation: Yu, K.; Zhang, Y.; Zhang, S.; Gao, M. Effects of $Al_2O_3/TiO_2/Na_2O$ on Lime Dissolution in Steelmaking Slag. *Metals* **2023**, *13*, 209. https://doi.org/10.3390/met13020209

Academic Editors: Alexander McLean and Rodolfo Morales

Received: 14 November 2022
Revised: 12 January 2023
Accepted: 17 January 2023
Published: 20 January 2023

Copyright: © 2023 by the authors. Licensee MDPI, Basel, Switzerland. This article is an open access article distributed under the terms and conditions of the Creative Commons Attribution (CC BY) license (https://creativecommons.org/licenses/by/4.0/).

$3CaO{\cdot}SiO_2$ layers formed only around the granular crystals instead of the continuous CaO crystals, which promoted the dissolution of lime. Evans and Deng et al. [11–13] studied the dissolution mechanism of lime in different liquid BOF slags containing CaO–FeO–SiO_2. They found that lime reacted with silicon dioxide in the slag, and a solid C2S calcium silicate layer formed at the interface between lime and the liquid slag. It has also been shown that CaO dissolved faster in the presence of a higher FeO content, as FeO penetrates the lime and facilitates the separation of the calcium silicate layer. Conversely, the C2S layer is dense when the FeO content decreases. This layer protects the lime from slag penetration, thereby reducing the dissolution rate.

However, comparative studies on the effects of $Al_2O_3/TiO_2/Na_2O$ on lime dissolution and their underlying mechanisms remain limited. Therefore, this study investigated the dissolution rate, solubility, and diffusion coefficient of CaO in $Al_2O_3/TiO_2/Na_2O$ slag, as well as the kinetic parameters for CaO dissolution. Additionally, the mechanisms of lime dissolution in slag in the presence or absence of $Al_2O_3/TiO_2/Na_2O$ were compared and discussed, providing important guidance for using red mud waste from alumina production as a steelmaking flux.

2. Experimental Methods

2.1. Materials and Slag Preparation

To obtain the active lime cylinder sample required for the test, 12 g of analytically pure CaO (Sinoreagent, Suzhou, China) was used as raw material. First, CaO was crushed into powder form. Thereafter, it was bonded with water and an organic binder, and pressed into a lime hollow cylinder (outside diameter = 20 mm, inner diameter = 7 mm, height = 20 mm, and pressure = 30 MPa) for 3 min. The lime cylinder was then dried in a resistance furnace at 1200 °C for 120 min to obtain an active lime column with a density between 1.46 and 1.50 g/cm^3 (Figure 1a). Then, the size of the dried lime cylinder was: outside diameter = 20 ± 1 mm, inner diameter = 7 ± 1 mm, height = 20 ± 1 mm.

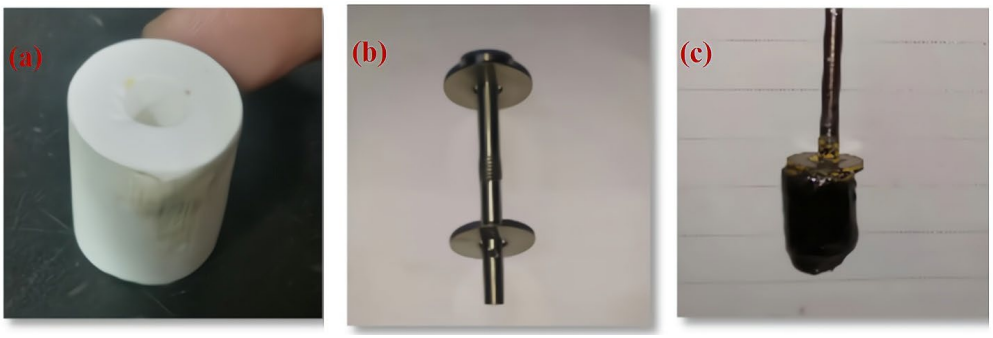


Figure 1. Preparation of the lime column. (**a**) Lime column after roasting; (**b**) molybdenum rotor; (**c**) lime column at the end of the experiment.

The slag used in this study was synthesized from analytical reagents. In the experiment, Na_2O and P_2O_5 were replaced with anhydrous sodium silicate and calcium phosphate, respectively. All the experimental chemical compositions are listed in Table 1. Sample 0 was the blank slag CaO–SiO_2–FeO–MgO–P_2O_5; Samples A, T, and N were composed of slag with 10% Al_2O_3, TiO_2, and Na_2O, respectively; Sample AT was a slag with 5% Al_2O_3 and 5% TiO_2; Sample AN was a slag with 5% Al_2O_3 and 5% Na_2O. Sample ATN was a slag with Al_2O_3:TiO_2:Na_2O = 15:4:3 (this ratio represents the composition of the slag after adding red mud from one factory). As lime dissolution mainly occurs in the early stage of converter steelmaking, the initial basicity of all slags was set to 1, and the reaction temperature was set to 1400 °C.

Table 1. Experimental materials (wt.%).

Sample	CaO	SiO_2	FeO	Al_2O_3	TiO_2	Na_2O	MgO	P_2O_5
0	36	36	20	0	0	0	5	3
A	31	31	20	10	0	0	5	3
T	31	31	20	0	10	0	5	3
N	31	31	20	0	0	10	5	3
ATN	31	31	20	6.8	1.8	1.4	5	3
AT	31	31	20	5	5	0	5	3
AN	31	31	20	5	0	5	5	3

2.2. Experimental Apparatus and Methods

Figure 1a shows the lime after roasting, and Figure 1b shows the molybdenum rotor. Molybdenum washers were present on the upper and lower sides of the lime column. Figure 1c shows the lime column at the end of the experiment. The dissolution experiments were conducted with the rotating disk apparatus shown schematically in Figure 2. This experiment used a vertical silicon–molybdenum furnace as the heating device, and the thermocouple was calibrated before the experiment. The protective gas used in this experiment was high-purity argon.

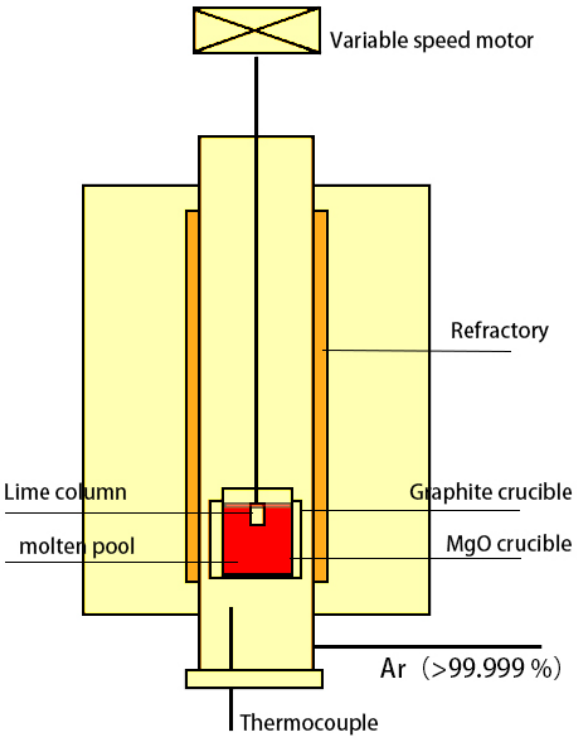


Figure 2. Experiment equipment.

First, 170 g of the slag sample was placed into the magnesia crucible (inside diameter = 60 mm, outer diameter = 70 mm, height = 100 mm). According to the temperature curve in Figure 3, the slag was heated to 1400 C by using a tube furnace (Baotou Yunjie Electric Furnace Factory, Baotou, China). After the slag sample was melted and the temperature remained constant at the target value, the lime column was slowly placed into the slag. The motor was immediately started and rotated at a speed of 150 rpm/min. Depending on the time required to completely dissolve the lime column, each group of experiments was performed four times for 3, 5, 10, or 15 (20) min—for the experiment with complete dissolution at 20 min, the data point obtained at 15 min was used.

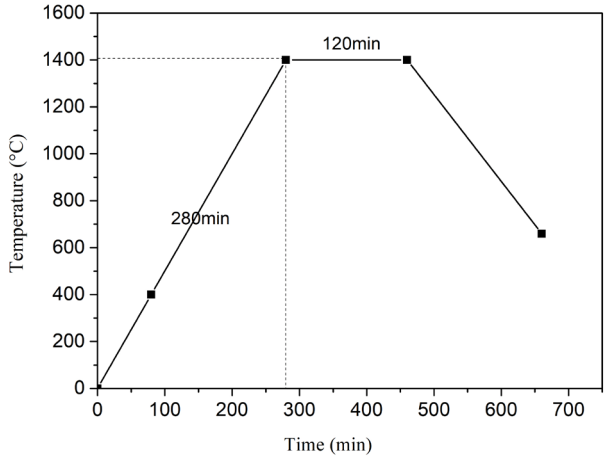


Figure 3. Temperature curve of the tube furnace.

After the experiment, the lime column was immediately lifted out of the slag, and the slag that adhered to the surface was shaken off at a high speed. Thereafter, the sample was removed from the furnace mouth, and the diameters of the different parts were directly measured using a digital vernier caliper (DEGUQMNT, Shanghai, China) at a high temperature. A horizontal plate was used to take pictures, and the average diameter value was used to calculate the reduction value of the sample diameter. After the experiment, a sample of the final slag was subjected to X-ray fluorescence analysis to calculate the amount of lime dissolved in the slag. After the lime dissolved, the lime column was mounted and polished in epoxy resin. It was then sprayed with gold, and the lime/slag interface was observed using scanning electron microscopy (SEM) (FEI, Portland, OR, USA) and chemically analyzed using energy dispersive spectrometry (EDS).

2.3. Analysis

As shown in Figure 1b, molybdenum washers were placed on the upper and lower sides of the lime column to protect them from contact with the slag; hence, the dissolved matter was concentrated on the side. The lime dissolution ratio X is defined as:

$$X = 1 - \frac{r_c}{r_0}\% \quad (1)$$

where r_0 and r_c are the initial and residual radii of the lime column, respectively.

To measure the dissolution rate of lime in slag, the experiment was characterized by the change of unit time radius of the lime column in slag, and the dissolution rate was:

$$v_r = -\frac{1}{S}\frac{dV}{dt} = -\frac{dr}{dt} \quad (2)$$

where v_r is the dissolution rate of the lime, m/s; V is the volume of the lime column, m^3; S is the side area of the lime column, m^2; and r is the radius of the lime column, m.

3. Results and Analysis

3.1. Effects of Al_2O_3, TiO_2, Na_2O, and ATN on the Dissolution Rate of Lime

Figure 4 shows the effects of adding different types of slag on the dissolution of lime. The results show that the addition of Al_2O_3, TiO_2, and Na_2O promoted the dissolution of lime. The lime dissolved fastest in Sample N (10% Na_2O) (50% lime dissolution was observed within 5 min, and 90% dissolution was achieved within 10 min). Sample T (10% TiO_2) dissolved the lime faster than Sample A (10% Al_2O_3), with 100% of the lime dissolved after 15 min. Sample 0, without additives, showed the slowest dissolution percentages, with only 52% of the lime column dissolved in 20 min. The dissolution of lime in Sample AN ($CaO–SiO_2–FeO–MgO–P_2O_5–5\%Al_2O_3–5\%Na_2O$) with 5% Na_2O was significantly

faster than that in Sample AT ($CaO–SiO_2–FeO–MgO–P_2O_5–5\%Al_2O_3–5\%TiO_2$). Additionally, lime dissolution was faster in Sample ATN ($CaO–SiO_2–FeO–MgO–P_2O_5–6.8\%Al_2O_3–1.8\%TiO_2–1.4\%Na_2O$) than in Samples AN and AT.

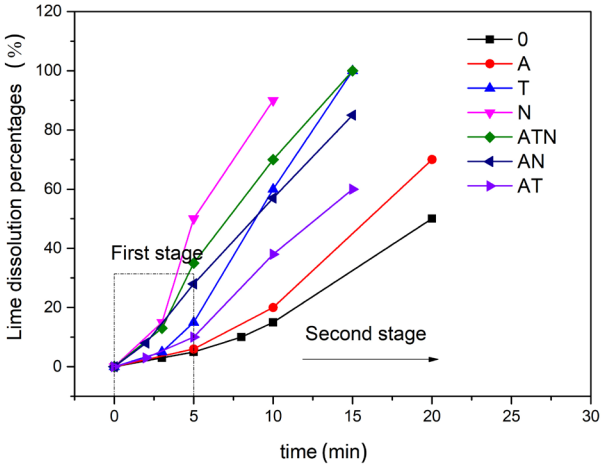


Figure 4. Dissolution percentages of lime in different slag samples.

Figure 4 shows that with the exception of Na_2O-bearing samples N, AN, and ATN, the dissolution process of lime in the analyzed samples can be profiled into two different stages: slow dissolution for the first 5 min and rapid dissolution after 5 min. The dissolution percentages of lime in the slag samples over 5 and 10 min are shown in Figure 5. The slow first stage is ascribed to the cooling of the nearby slag upon contact with the lime column, which reduces its fluidity and results in the slow dissolution of lime. No distinct first stage is observed for the samples containing Na_2O because it can significantly reduce the melting point of the slag. In the second stage, which occurs after the first 5 min, the lime dissolution rate varied linearly with time, which is consistent with previously reported findings [14].

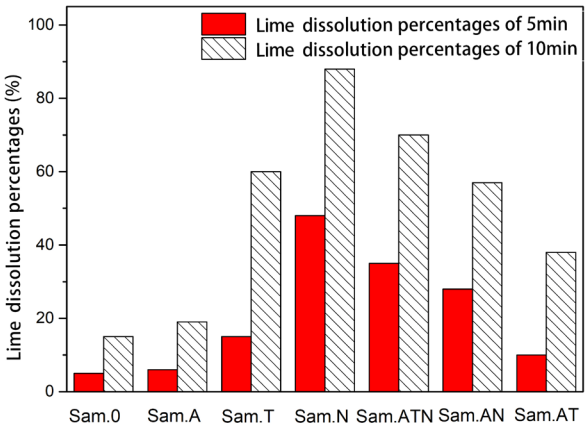


Figure 5. Dissolution percentages of lime in slag after 5 and 10 min.

The dissolution rate of lime was calculated based on the linear fitting of the second dissolution stages, as presented in Table 2, with a fitting degree R^2 above 0.9. Figure 6 shows a comparison between the experimental lime dissolution rates obtained here and those reported in the literature. Comparing samples containing 10% Al_2O_3, the v_r/v_0 for sample A closely matched those reported by Diao [15], Guo et al. [16], and Sarkar [17], whereas Sample ATN showed a higher dissolution rate. In samples containing Na_2O, the v_r/v_0 value for sample N was higher than the values reported by Diao [15] and Guo et al. [16]. It is possible that sodium oxide significantly reduces the viscosity at higher temperatures, thus accelerating the dissolution of lime.

Table 2. Dissolution rate of lime (10^{-5} cm/s).

Sample	0	A	T	N	ATN	AN	AT
Second stage v_r	2.77	3.93	7.69	9.75	8.08	6.65	5.83

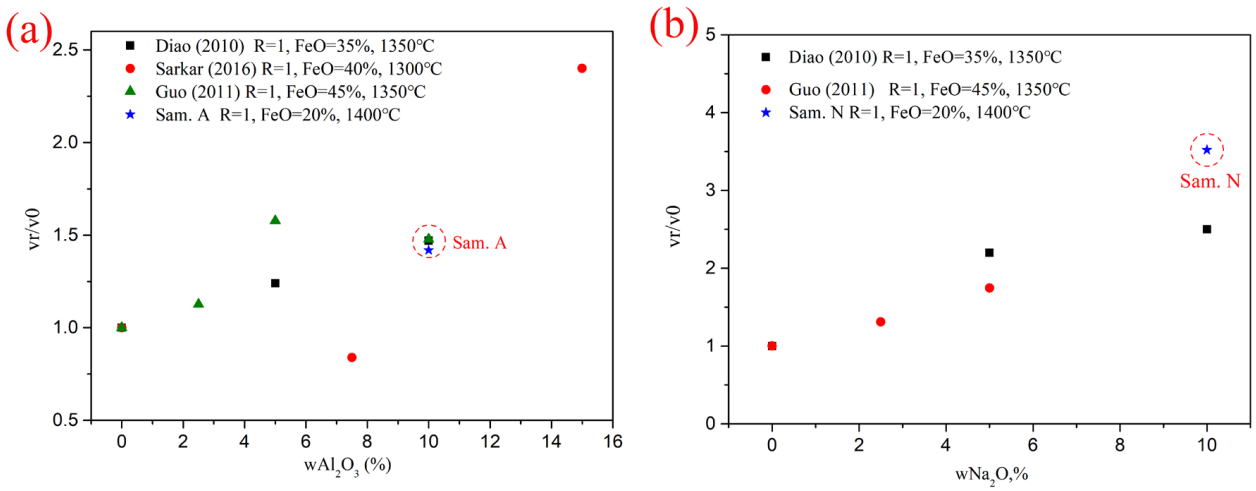


Figure 6. Comparison of dissolution rates of lime in the existing literature with experimental dissolution rates obtained here ((**a**) add Al_2O_3 [15–17], (**b**) add Na_2O [15,16]) (v_r is the lime dissolution rate after adding $Al_2O_3/TiO_2/Na_2O$; v_0 is the lime dissolution rate before adding $Al_2O_3/TiO_2/Na_2O$).

To quantitatively evaluate the effect of adding $Al_2O_3/TiO_2/Na_2O$ to promote the dissolution of lime into the CaO–SiO_2–FeO–MgO–P_2O_5 slag, A is defined as the promotion coefficient, which is the promotion of unit $Al_2O_3/TiO_2/Na_2O$ content to the dissolution rate of lime in the original slag system. The formula is calculated as follows:

$$A = \frac{v_r - v_0}{\%X} \quad (3)$$

where v_0 and v_r, respectively, are the lime dissolution rates (cm/s) before and after adding $Al_2O_3/TiO_2/Na_2O$, and X is the percentage of added $Al_2O_3/TiO_2/Na_2O$.

Based on the promotion coefficients listed in Table 3, the promotion effect of Na_2O on lime dissolution in slag is larger than that of Al_2O_3. Therefore, adding only a small amount of Na_2O can substantially increase the dissolution of lime. The values obtained for promotion coefficients can be used in actual production.

Table 3. Promotion coefficients of the dissolution rate of lime with different additives (cm/s).

Promotion Coefficient Units	Al_2O_3	TiO_2	Na_2O
A	1.162×10^{-6}	4.917×10^{-6}	6.98×10^{-6}

3.2. Effects of Al_2O_3, TiO_2, Na_2O, and ATN on Structure in Lime Dissolution

Figure 7a–e show SEM images of the microstructure and the phase composition of the interface between lime and slag after 10 min dissolution of sample 0, A, T, N, ATN in lime. Based on SEM and EDS analyses, four types of phases are generated near the interface during lime dissolution, in addition to the initial slag and lime (Table 4): Phase 1 is slag; phase 2 (C2S) contains Ca_2SiO_4 and other silicate phases; phase 3 (MF) is the boundary layer, with a high content of Fe and Mg; phase 4 (CF) is intrusive slag, which is the slag that has invaded the pores of the lime and is a high iron-containing phase that comprises compounds such as calcium ferrite; phase 5 is residual solid lime; and phase 6 is a Ti-containing phase with compounds such as $CaTiO_3$ and $CaSiTiO_5$. The elemental

composition of each phase for Samples 0, A, T, N and ATN was determined through an EDS analysis (Table 4).

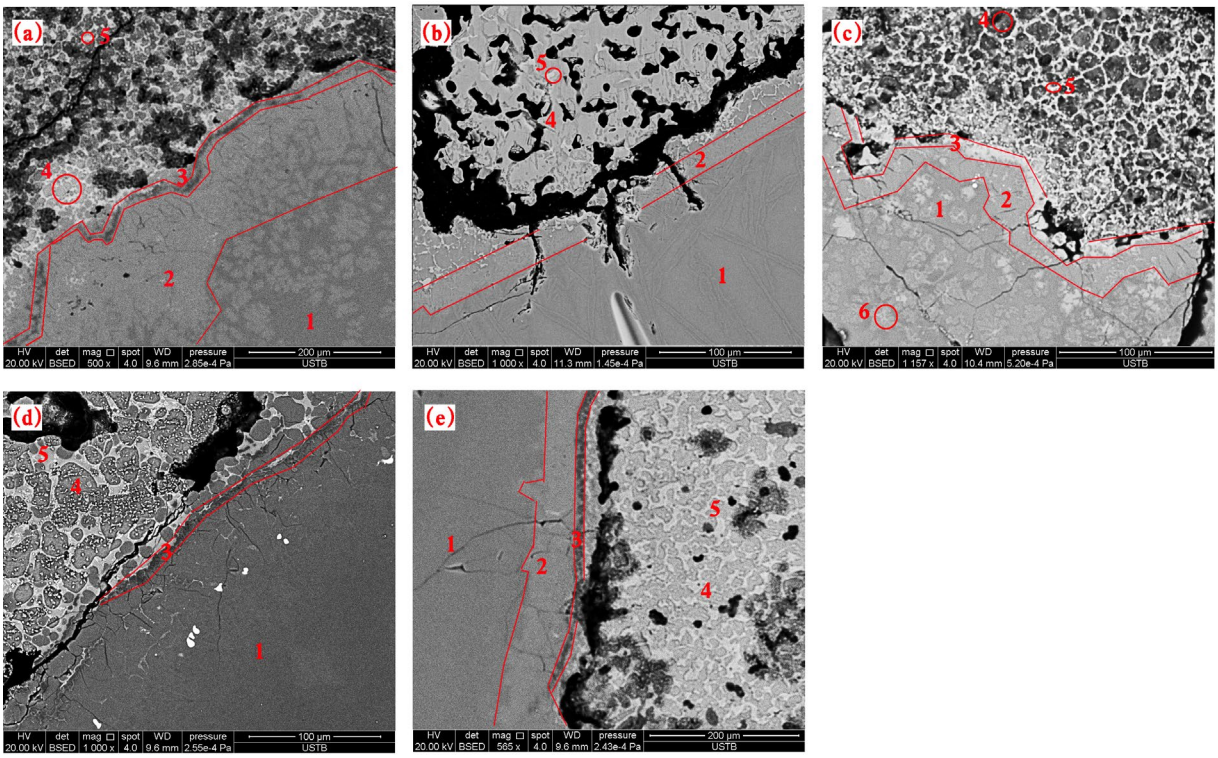


Figure 7. Microstructure and phase composition of lime samples with slag. ((**a**) Sample 0, (**b**) Sample A, (**c**) Sample T, (**d**) Sample N, and (**e**) Sample ATN; 1: slag, 2: C2S, 3: MF, 4: CF, 5: lime, 6: Ti-containing).

Table 4. EDS analysis results (wt.%).

Sample	Main Phase	Al	Mg	Si	P	Ca	Fe	Na	Ti	O
0	2-C2S	-	-	13.14	-	24.38	3.73	-	-	57.33
	3-MF	-	29.39	-	-	1.46	20.09	-	-	49.05
	4-CF	-	-	-	-	20.38	19.8	-	-	57.83
	5-lime	-	-	-	-	35.17	3.75	-	-	55
A	2-C2S	4.18	0.72	16.07	0.38	17.69	-	-	-	61.97
	4-CF	5.2	1.71	-	-	17.74	18.55	-	-	56
	5-lime	-	-	-	-	42.33	-	-	-	57.66
T	2-C2S	-	1.94	16.81	-	16.25	2.57	-	4.89	59.22
	3-MF	-	29.39	-	-	1.46	20.09	-	-	49.05
	4-CF	-	1.44	-	-	17.63	27.59	-	-	53.34
	5-lime	-	-	-	-	43	-	-	-	57
	6-Ti-containing	-	-	8.37	-	41.21	-	-	14.27	36.15
N	3-MF	-	13.42	-	-	1.89	58.24	-	-	26.45
	4-CF	-	1.53	-	0.46	25.39	13.64	1.48	-	56.70
	5-lime	-	-	-	-	34.99	-	-	-	65.01
ATN	2-C2S	7.87	3.33	12.46	-	35.95	8.81	0.74	-	30.83
	3-MF	-	15.45	5.00	-	26.89	30.89	-	-	21.77
	4-CF	6.73	1.91	1.59	-	26.89	33.70	0.13	-	21.05
	5-lime	-	-	-	-	49.01	4.71	-	-	46.28

The phases that were identified in each sample were compared with the theoretical phases in lime dissolution, as calculated using FactSage 7.0 (Figure 8). Sample 0 contains phases (1)–(5). Figure 7b shows that no new phase formed after the addition of Sample A slag, and the absence of the MF phase on the boundary is observed. This is in agreement with calculations by Michelic [18] and the predictions by FactSage (Figure 8b). Owing to a combination of structural and dissolution rate changes, Al was mainly present in the slag and in the MF boundary layer. The formation of $Ca_2Al_2SiO_7$ reduced the CaO concentration at the interface between the slag and the lime column. Moreover, the calcium ferrite content in the pores of Sample A was lower than those of samples T and ATN and was equivalent to that in Sample 0.

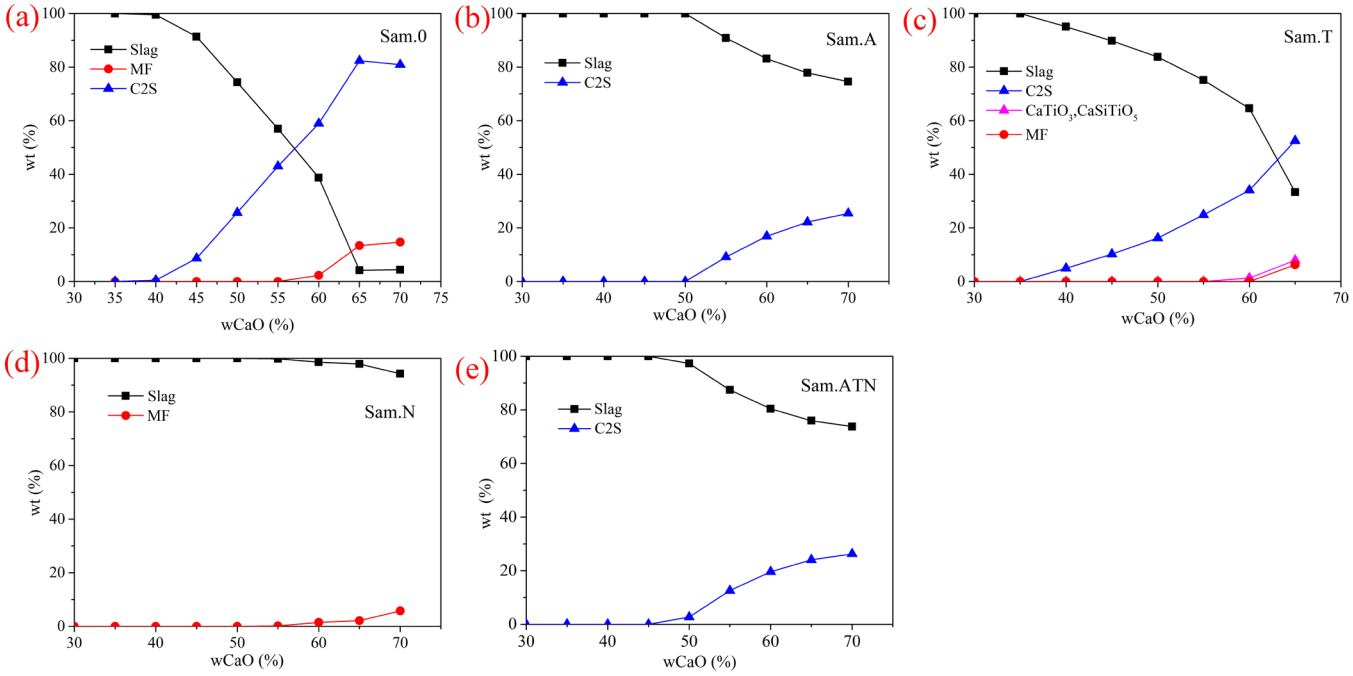


Figure 8. Theoretical phases in lime dissolution calculated by FactSage 7.0. ((**a**) Sample 0, (**b**) Sample A, (**c**) Sample T, (**d**) Sample N, (**e**) Sample ATN).

Figure 7c indicates that after adding 10% TiO_2, a phase containing $CaTiO_3$ and $CaSiTiO_5$ phase was formed in Sample T. This phase was also predicted by the FactSage calculations. As the dissolution rate changed, the Ti-containing phase consumed the C2S layer and CaO near the slag boundary, which accelerated mass transfer, as well as the rate of breakthrough of the C2S layer in lime dissolution and dissolution rate in the first stage. Ti-containing phases in the slag, such as $CaTiO_3$ and $CaSiTiO_5$, were also reported in the FeOx–SiO_2–V_2O_3–TiO_2 slag system by Tang R [19]. As presented in Table 4, unlike Al in Sample A, Ti was not detected in the boundary layer or the lime gap of Sample T. Compared with Sample 0, after adding TiO_2 for 10 min, the Fe content in the CF increased to 27.59%. The increased content of calcium ferrite in the lime pores promoted lime dissolution.

Figure 7d shows the SEM images of the microstructure and phase composition for Sample N. Compared with Sample 0, the C2S layer was absent from the interface between the slag and lime, suggesting that the addition of 10% Na_2O hindered the formation of the C2S layer and improved the mass transfer coefficient (k) of CaO in the lime column. This also explains the reason for not observing the first stage of lime dissolution in Samples N and AN. The EDS analysis of Sample N indicated that the addition of Na_2O promoted the transfer of Fe from the slag to the boundary layer. As the dissolution time increased to 10 min, the Fe content in the boundary layer increased to 58.24%, which was more than double compared to those in samples 0, A, and T.

Figure 7e and Table 4 present the phase changes in slag and the dissolution of lime after adding 10% ATN. No prominent new phases are observed. Both Al and Na are found in the slag and invading lime cracks, and Ti is not detected because the added TiO_2 content is only 1.8%. The Fe content in the intrusive phase is 33.7%, which is higher than those in samples 0, A, and T, indicating that adding ATN also promotes the rapid dissolution of lime. Therefore, the dissolution rates in the first and second stages for sample ATN are higher than those following the addition of Al_2O_3 or TiO_2.

4. Discussion

4.1. Dissolution Process of Lime in Slag

The dissolution process of the active lime column in the slag sample 0 as observed during the experiment is shown in Figure 9. After leaching the active lime, the slag penetrated the lime along the pores/cracks. With increased exposure time, the black layer thickened, and then, the metamorphic lime column started to dissolve in the slag.

$$(CaO) + (FeO) \rightarrow (CaO{\cdot}FeO) \quad (4)$$

$$(MgO) + (FeO) \rightarrow (MgO{\cdot}FeO) \quad (5)$$

$$2(CaO) + (SiO_2) \rightarrow (2CaO{\cdot}SiO_2) \quad (6)$$

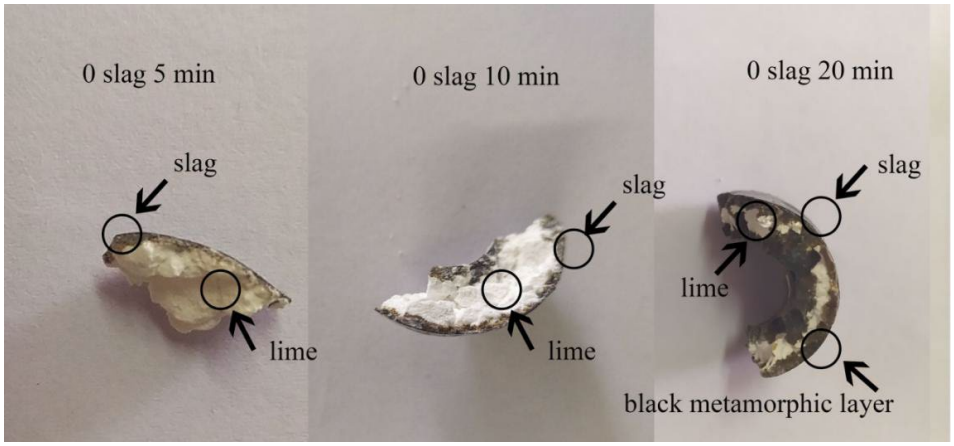


Figure 9. Dissolution process of lime in Sample 0 slag.

As shown in Figure 10, combining the EDS, SEM, and FactSage calculation results, the dissolution process of lime in the $CaO–SiO_2–FeO–MgO–P_2O_5$ converter slag system is as follows:

1. FeO enters lime pores and forms calcium ferrite and diffuses (Equation (4)). The formation of calcium ferrite causes the lime column to further break apart, which increases the dissolution rate of active lime.
2. The reaction in Equation (5) occurs at the boundary of the lime column, generating an intermittent MF layer.
3. CaO passes through the CF phase and then through the gap in the MF phase. The reaction in Equation (6) occurs to form the C2S phase, and the dense C2S layer prevents FeO from further entering the lime.
4. CaO diffusion into the slag occurs through the boundary layer.
5. This mechanism is reflected in the findings of Deng, Guo, and Chen [12,14,20]. Therefore, we investigated the effect of adding $Al_2O_3/TiO_2/Na_2O$ on the stages of the dissolution process.

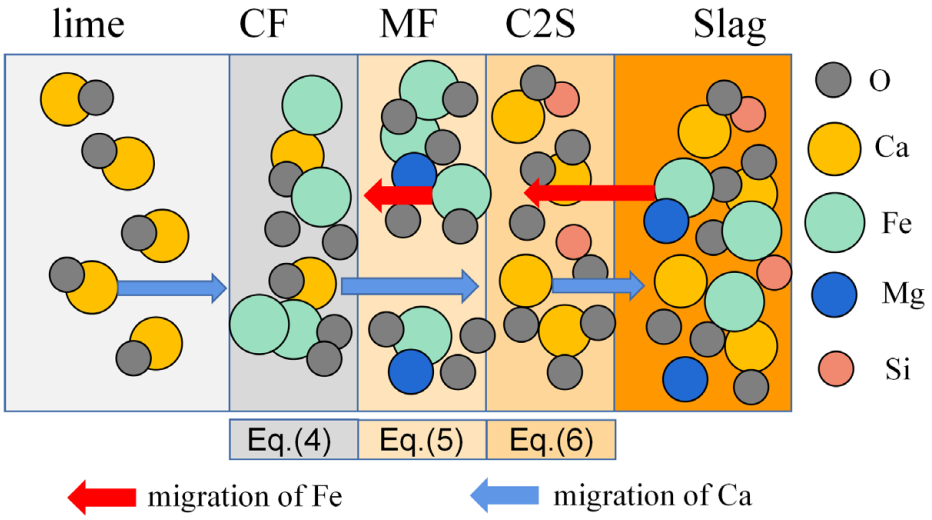


Figure 10. Diagram of the dissolution process of the lime column.

4.2. Effects of Al_2O_3, TiO_2, and Na_2O on the Lime Dissolution Process in Slag

The addition of Al_2O_3/TiO_2/Na_2O influences the dissolution rate of lime in two major aspects: it affects the formation of different phases as well as the diffusion speed of CaO in the slag.

Figure 11 demonstrates the phase changes during lime dissolution in the Al_2O_3/TiO_2/Na_2O–CaO–SiO_2–FeO–MgO–P_2O_5 slag system. The MF and C2S layers hinder the diffusion of CaO during lime dissolution. In sample A, with the addition of 10% Al_2O_3, the boundary layer of MF disappears, and CaO diffusion is accelerated. In Sample T, after the addition of TiO_2, $CaTiO_3$ and $CaSiTiO_5$ phases are formed in the slag. In sample N, after the addition of Na_2O to the slag, the C2S layer disappears, and CaO dissolution is accelerated.

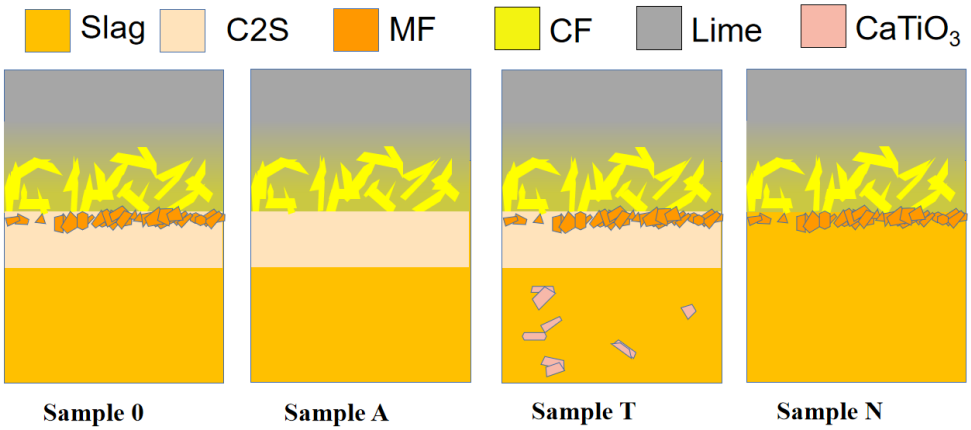


Figure 11. Phase change diagram for lime dissolution.

The dissolution rates of lime in the second stage are shown in Figure 12. For each slag used in the experiment, viscosity at 1400 °C was calculated based on the viscosity model proposed by Zhang [21–25] (Figure 12).

Compared with sample 0, after adding Al_2O_3, the MF boundary layer disappears in Sample A, which accelerates the dissolution of lime. However, the increase in viscosity caused by Al_2O_3 impedes CaO diffusion in slag, eventually leading to only a slight increase in the lime dissolution rate.

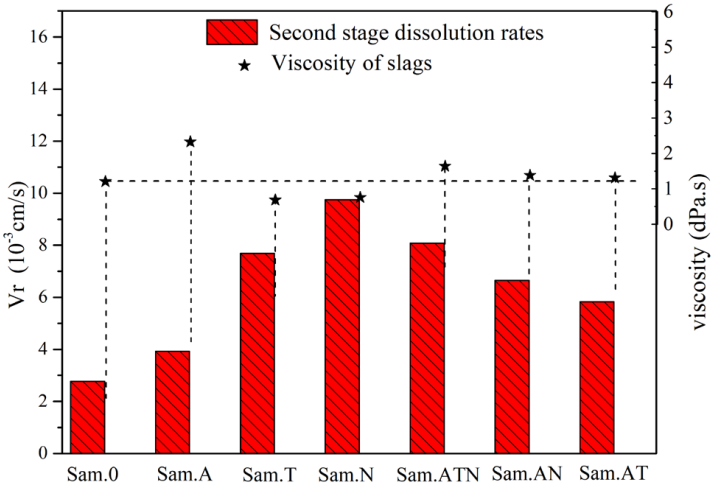


Figure 12. Dissolution rates of lime and viscosity in different slags in the second stage.

In sample T with 10% TiO_2, $CaTiO_3$ and $CaSiTiO_5$ are generated in the slag, which increases the diffusion coefficient k of CaO in slag. Additionally, the reduction in viscosity facilitates the mass transfer of CaO and promotes lime dissolution.

In Sample N, after the addition of Na_2O, the C2S layer disappears, and the viscosity of the slag is significantly reduced. These factors facilitate the mass transfer of CaO and significantly accelerate the dissolution of lime.

Na_2O had a beneficial effect on accelerating the dissolution of lime. However, an excessive Na_2O content will cause the corrosion of refractory materials and adversely affect the continuous operation of the converter. At present, the Na_2O content in the slag after using red mud as flux is less than 1.5%, so the use of limited amount of red mud will not aggravate the erosion of refractory [2,3].

4.3. Effects of Al_2O_3, TiO_2, and Na_2O on Dissolution Kinetics of Lime

Focusing on the chemical reaction control process, the diffusion mass transfer of CaO in the boundary layer is a control process in which the slag dissolves the lime under a forced flow [14,26,27]. To evaluate the k of lime in slag, the dissolution rate of lime is first determined as follows:

$$J = \rho_L \cdot v_r, \tag{7}$$

where J is the dissolution rate of lime expressed using mass (g/cm^2·s); ρ_L is the density of the lime column (g/cm^3); and v_r is the dissolution rate of lime (m/s). J is used to calculate k based on the following equation:

$$J = k(n_s - n_b), \tag{8}$$

where k is the mass transfer coefficient (cm/s); n_s and n_b are the CaO contents in the interface and slag body, respectively (g/cm^3).

$$v_r = \frac{k}{100\rho_L}(c_s\rho_s - c_b\rho_b) \approx \frac{k\rho_b}{100\rho_L}(c_s - c_b) = \frac{k\rho_b}{100\rho_L}\Delta w(CaO) \tag{9}$$

$$k = \frac{100 v_r \rho_L}{\rho_b \Delta w(CaO)} \tag{10}$$

ρ_s and ρ_b are the slag density and slag packing density (g/cm^3) at the interface between the lime and slag, respectively. ρ_b was measured using the DP-300P drainage density tester after slag quenching to obtain the slag density at 1400 °C, as listed in Table 5; c_s is the concentration of CaO at the interface between the surface of decomposed CaO and molten slag (mol·m^{-3}) and can be determined from the intersection of the liquidus

line with a straight line connecting the point of bulk slag composition and the CaO apex on the CaO–SiO_2–FeO–MgO–P_2O_5–Al_2O_3/TiO_2/Na_2O phase diagram [27]; c_b is the bulk concentration of (CaO) in molten slag (mol·m^{-3}); the calculated Δw (CaO) = $c_s - c_b$ is listed in Table 5. ρ_L is the density of the lime column, 1.48 g/cm^3.

Table 5. Kinetic parameters for lime dissolution in slag.

Slag	0	A	T	N	ATN
K (cm/s)	0.445×10^{-4}	1.205×10^{-4}	2.279×10^{-4}	4.123×10^{-4}	2.373×10^{-4}
ρb (g/cm^3)	3.7	3.06	3.58	3.1	3.12
Δw (CaO)	11.1%	15.78%	13.94%	11.29%	16.15%

Using the aforementioned equations, the k values of CaO under different conditions were calculated.

K values for the CaO–SiO_2–FeO–MgO–P_2O_5–Al_2O_3/TiO_2/Na_2O slag at 1400 °C ranged between 0.445×10^{-4} and 4.123×10^{-4} cm/s. The addition of Al_2O_3, TiO_2, and Na_2O significantly increased the k of the slag and reduced the thickness of the boundary layer. After the addition of 10% Al_2O_3 and TiO_2, the k of the slag increased to 1.205×10^{-4} and 2.279×10^{-4} cm/s, respectively. After the addition of 10% Na_2O, k increased to 4.123×10^{-4} cm/s. The addition of Al_2O_3, TiO_2, and Na_2O in slag significantly promoted the dissolution of lime in the converter.

5. Conclusions

1. When 10% Al_2O_3/TiO_2/Na_2O was added to a CaO–SiO_2–FeO–MgO–P_2O_5 slag, Al_2O_3, TiO_2, and Na_2O showed promoting effects on the dissolution of lime under forced-convection molten pool mixing. The effect of additives on slag increased in the order of Al_2O_3 < TiO_2 < Na_2O, with promotion coefficients of 1.162×10^{-6}, 4.917×10^{-6}, and 6.98×10^{-6} cm/s·%, respectively.
2. The addition of Al_2O_3 caused the disappearance of the MF layer and increased the viscosity of the slag, which led to a slight overall increase in the dissolution rate of lime. TiO_2 generated a new phase containing $CaTiO_3$ and $CaSiTiO_5$ in the slag, and reduced its viscosity, promoting lime dissolution. The addition of Na_2O caused the C2S layer to disappear, as well as significantly reduced the viscosity of slag and accelerated lime dissolution.
3. The kinetic parameters of the Al_2O_3/TiO_2/Na_2O–CaO–SiO_2–FeO–MgO–P_2O_5 slag at 1400 °C and 150 rpm were calculated. Al_2O_3/TiO_2/Na_2O significantly increased the k of the slag, and the promotion coefficients increased to 4.123×10^{-4} m/s after 10% Na_2O was added. The addition of red mud-based additives containing a mixture of Al_2O_3, TiO_2, and Na_2O can effectively increase the dissolution rate of lime, and the promotion ability is higher than that obtained by individually adding the same content of Al_2O_3 and TiO_2. This suggests that red mud may be a suitable flux for application in the steelmaking industry, but the amount added during steelmaking should also be limited.

Author Contributions: Conceptualization, K.Y. and Y.Z.; writing—original draft preparation, K.Y.; supervision, S.Z. and M.G. All authors have read and agreed to the published version of the manuscript.

Funding: Financial support for this work was provided by the National Key R&D Program of China (2019YFC1905701) and National Natural Science Foundation of China (52204336), which is acknowledged with gratitude.

Data Availability Statement: Not applicable.

Conflicts of Interest: The authors declare no conflict of interest.

References

1. Pretorius, E. *Fundamentals of EAF and Ladle Slags and Ladle Refining Principles*; Bakers Refractories: York, PA, USA, 2015. Available online: https://www.academia.edu/34134047/FUNDAMENTALS_OF_EAF_AND_LADLE_SLAGS_AND_LADLE_REFINING_PRINCIPLES (accessed on 13 November 2022).
2. Zhang, Y.; Li, F.; Wang, R.; Tian, D. Application of Bayer Red Mud-Based Flux in the Steelmaking Process. *Steel Res. Int.* **2016**, *88*, 304–313. [CrossRef]
3. Zhang, Y.; Li, F.; Yu, K. Using Red Mud-based Flux in Steelmaking for High Phosphorus Hot Metal. *ISIJ Int.* **2018**, *58*, 2153–2155. [CrossRef]
4. Shiro, B.Y.; Mitsutaka, H.; Retsu, N.; Nagabayashi, R. Dephosphorization and Desulphurization of Hot Metal with CaO-Al_2O_3-Fe_xO_y Flux. *Tetsu-to Hagané* **2009**, *75*, 66–73.
5. Mukawa, S.; Mizukami, Y. The Rate of Hot Metal Desulfurization by Na_2O-CaO Flux. *Tetsu-to-Hagané* **1996**, *82*, 659–664. [CrossRef] [PubMed]
6. Mukawa, S. Effect of flux composition on the rate of desulfurization of hot metal by CaO-Al_2O_3 flux. *Tetsu-to-Hagané* **2004**, *90*, 408–413. [CrossRef]
7. Shimoda, I.; Sato, T.; Nakasuga, T. Effect of oxide additives on desulfurization efficiency of hot metal by CaO-based powders. *Tetsuto-Hagané* **2004**, *90*, 401–407. [CrossRef]
8. Lee, M.; Barr, P. The properties and production of iron-coated burnt lime. *Steel Res.* **2002**, *73*, 123–128. [CrossRef]
9. Hamano, T.; Horibe, M.; Ito, K. The dissolution rate of solid lime into molten slag used for hot-metal dephosphorization. *ISIJ Int.* **2004**, *44*, 263–267. [CrossRef]
10. Schlitt, W.J.; Healy, G.W. Kinetics of lime dissolution in CaO-FeO-SiO_2 slags. *Am. Ceram. Soc. Bull.* **1971**, *50*, 954–960.
11. Natalie, C.A.; Evans, J.W. Influence of Lime Properties on Rate of Dissolution in CaO-SiO_2-FeO Slags. *Ironmak. Steelmak.* **1979**, *6*, 101–109.
12. Deng, T.; Gran, J.; Sichen, D. Dissolution of Lime in Synthetic FeO-SiO_2 and CaO-FeO-SiO_2 Slags. *Steel Res. Int.* **2010**, *81*, 347–355. [CrossRef]
13. Deng, T.; Sichen, D. Study of lime dissolution under forced convection. *Metall. Mater. Trans. B* **2012**, *43*, 578–586. [CrossRef]
14. Guo, X.L.; Sun, Z.H. In Situ Observation on Lime Dissolution in Molten Metallurgical Slags–Kinetic Aspects. *Ind. Eng. Chem. Res.* **2014**, *53*, 6325–6333. [CrossRef]
15. Diao, J.; Wang, Y.H.; Guo, X. Effect of Fluorine on the Minerals Phase and Citric Acid Solubility of CaO-SiO_2-Fe_tO-P_2O_5-CaF_2 System. *ISIJ Int.* **2010**, *50*, 768–770. [CrossRef]
16. Guo, X. Study on Lime Dissolution Behavior of Converter Duplex Dephosphorization Furnace. Master's Thesis, Chongqing University, Chongqing, China, 2011.
17. Sarkar, R.; Roy, U.; Ghosh, D. A Model for Dissolution of Lime in Steelmaking Slags. *Metall. Mater. Trans. B* **2016**, *47*, 2651–2665. [CrossRef]
18. Michelic, S.K.; Bernhard, C. Experimental Study on the Behavior of TiN and Ti_2O_3 Inclusions in Contact with CaO-Al_2O_3-SiO_2-MgO Slags. *Scanning* **2017**, *2017*, 2326750. [CrossRef]
19. Tang, R.; Wang, Y.T.; Wang, S. Dissolution mechanism of lime in FeO_x-SiO_2-V_2O_3-TiO_2 slag. *Charact. Miner. Met. Mater.* **2013**, *2013*, 99–108. [CrossRef]
20. Chen, M.; Deng, H.H.; Wang, N. Limestone Dissolution in Converter Slag: Kinetics and Influence of Decomposition Reaction. *ISIJ Int.* **2018**, *58*, 2271–2279. [CrossRef]
21. Zhang, G.H.; Chou, K.C. Measuring and Modeling Viscosity of CaO-Al_2O_3-SiO_2(-K_2O) Mel. *Metall. Mater. Trans. B* **2012**, *43*, 841–848. [CrossRef]
22. Zhang, G.H.; Chou, K.C. Modelling Viscosities of CaO–MgO–Al_2O_3–SiO_2 Molten Slags. *Isij Int.* **2012**, *52*, 355–362. [CrossRef]
23. Zhang, G.H.; Chou, K.C. Influence of CaF_2 on viscosity of aluminosilicate melts. *Ironmak. Steelmak.* **2013**, *40*, 376–380. [CrossRef]
24. Zhang, G.H.; Chou, K.C. Correlation Between Viscosity and Electrical Conductivity of Aluminosilicate Melts. *Metall. Mater. Trans. B* **2012**, *43*, 849–855. [CrossRef]
25. Zhang, G.H.; Chou, K.C. Modeling Viscosities of CaO-MgO-FeO-MnO-SiO_2 Molten Slags. *Metall. Mater. Trans. B* **2012**, *43*, 64–72. [CrossRef]
26. Wang, Y.; Guo, X.; Xie, B. Kinetics of lime dissolution in converter dephosphorization slag. *J. Iron Steel Res.* **2011**, *23*, 8–10. [CrossRef]
27. Matsushima, M.; Yadoomaru, S.; Mori, K. Fundamental Study on the Dissolution Rate of CaO into Liquid Slag. *Tetsuto-Hagané* **1976**, *62*, 182.

Disclaimer/Publisher's Note: The statements, opinions and data contained in all publications are solely those of the individual author(s) and contributor(s) and not of MDPI and/or the editor(s). MDPI and/or the editor(s) disclaim responsibility for any injury to people or property resulting from any ideas, methods, instructions or products referred to in the content.